International Journal of Nanoscience
Vol. 7, No. 6 (2008) 333–338
© World Scientific Publishing Company

QUANTUM STATE DEPRESSION IN A SEMICONDUCTOR QUANTUM WELL

AVTO TAVKHELIDZE* and VASIKO SVANIDZE
Tbilisi State University, Chavchavadze Avenue 13
0179 Tbilisi, Georgia
*avtotav@geo.net.ge

Revised 15 October 2008

In this study, the quantum state depression (QSD) in a semiconductor quantum well (QW) is investigated. The QSD emerges from the ridged geometry of the QW boundary. Ridges impose additional boundary conditions on the electron wave function, and some quantum states become forbidden. State density is reduced in all energy bands, including the conduction band (CB). Hence, electrons, rejected from the filled bands, must occupy quantum states in the empty bands due to the Pauli exclusion principle. Both the electron concentration in the CB and the Fermi energy increased, as in the case of donor doping. Since quantum state density is reduced, the ridged quantum well (RQW) exhibits quantum properties at widths approaching 200 nm. A wide RQW can be used to improve photon confinement in QW-based optoelectronic devices. Reduction in the state density increases the carrier mobility and makes the ballistic transport regime more pronounced in the semiconductor QW devices. Furthermore, the QSD doping does not introduce scattering centers and can be used for power electronics.

Keywords: Quantum well; density of sates; optoelectronics; ballistic transport; Casimir effect.

1. Introduction

Quantum well (QW) lasers, solar cells, and transistors are fabricated based on semiconductor heterostructure technologies.[1] The typical thickness of the QW layer is 10–20 nm. A lower thickness is essential for reducing the density of the quantum states and realizing the quantum properties of the well. However, thin layers do not confine the photons (needed for optoelectronics) and do not carry high currents (needed for power electronics). Recently, quantum state depression (QSD) was investigated both theoretically[2] and experimentally.[3] QSD allows reduction of quantum state density and realization of quantum properties of the thick layer. It is based on the ridged geometry of the layer boundary. Periodic ridges impose additional boundary conditions on the electron wave function. Supplementary boundary conditions forbid some quantum states for free electrons, and the state density in k space $\rho(k)$ is reduced. Due to the Pauli exclusion principle, electrons rejected from the forbidden quantum states have to occupy the states with higher k. Thus, Fermi vector k_F and Fermi energy E_F increase. In semiconductors, QSD reduces $\rho(E)$ in all energy bands, including the conduction band (CB). Electrons, rejected from the filled bands, occupy the quantum states in the empty bands, and the electron concentration in the CB increases. This corresponds to donor doping. QSD depends on electron confinement and, therefore, is most pronounced in QW structures.

The objective of this work is to calculate the parameters of the semiconductor ridged quantum well (RQW) and discuss the possible applications. Initially, the basic features of QSD in semiconductors are described. Subsequently, the density of the quantum states in k space $\rho(k)$ and energy $\rho(E)$ for the RQW are evaluated and compared with

those of the conventional QW. The number of QSD-generated electrons is determined and the formulas for electron concentration and E_F are obtained. Furthermore, the charge transport in the RQW is analyzed and the formulas for carrier mobility and electrical conductivity are obtained. Finally, the advantages of using the RQW for optoelectronic devices and ballistic transport devices are discussed.

2. Semiconductor RQW

The cross-section of an RQW layer is shown in Fig. 1(a). There are periodic ridges having width w and height a on the surface of a conventional QW layer. Potential energy changes instantly, by value D, at the surface of all walls. Figure 1(b) shows a schematic representation of the corresponding potential well. The dashed line depicts the double right side boundary. In addition, the metal RQW was investigated in an earlier study.[2] Let us now find the distinctive features of the semiconductor RQW. Like in metals, the QSD forbids some quantum states. However, before going into their details, the distinctions and similarities between the QSD-forbidden state and a hole should be elucidated. The QSD-forbidden state is forbidden by the boundary conditions and cannot be occupied. However, it is not forbidden in an irrevocable way. If the boundary conditions change (e.g. due to charge depletion), then the QSD-forbidden state can recombine with the electron. As the QSD-forbidden state is confined to the boundary conditions (macroscopic geometry), it is not localized in the lattice and cannot move like a hole.

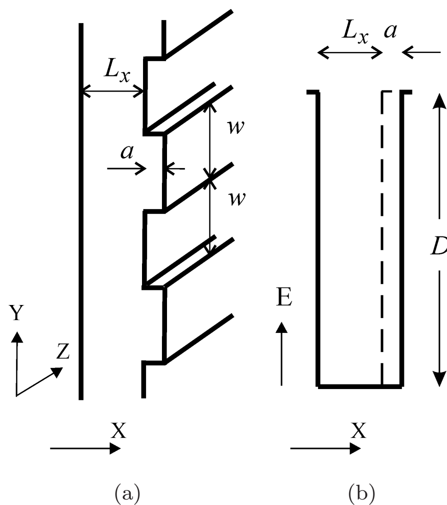

Fig. 1. (a) 3D view of the RQW; (b) schematic representation of the RQW.

The QSD transfers electrons to higher energy levels. If initially the semiconductor is of the p type, then the QSD will change it to an undoped or even to the n type. The QSD is comparable with a conventional donor doping, from the point of increase in E_F. However, there are no donor atoms in the case of QSD doping, which makes it akin to modulation doping. Unlike modulation doping, there is no space charge, as the QSD does not redistribute the charge and just transfers the electrons from the filled energy bands to the empty ones. Moreover, the material remains uniformly neutral.

It is convenient to make a comparison between the RQW and the QW. Furthermore, the main parameters — such as $\rho(k)$, $\rho(E)$, and E_F — of the RQW can be expressed in terms of the same parameters of the conventional QW ($a = 0$). It can be assumed that both the wells are made from the undoped material and are deep enough (to allow the limit of an infinitely deep well). $\rho(k)$ is inversely proportional to the volume of the k space elementary cell. The cell volume for the RQW can be found[2] on the basis of the volume perturbation method of solving the time-independent Schrödinger equation (Helmholtz equation).[4,5] However, this method can be used only when $a \ll L_x$. The RQW volume is divided into two parts: main volume (MV) and additional volume (AV). It is presumed that MV $\gg$ AV and it defines the form of the solutions for the whole RQW volume. Subsequently, the solutions of the RQW volume are searched in the form of solutions of the MV. The method is especially effective in the case where the MV has a simple geometry, e.g. rectangular geometry, allowing separation of the variables. In this study, the volume of the ridge was regarded as the AV having dimensions a, w, L_z. The MV had the dimensions L_x, L_y, L_z. Solutions were plane de Broglie waves with a discrete k spectrum. Further, the electron wave function and its derivative were matched from the two sides on the border of the MV and AV. The result obtained was the reduction of $\rho(k)$ and the increase of E_F in the RQW (a detailed description can be found in Ref. 2). Analysis was made within the limit of the quantum model of free electrons. Here, we extrapolate the results to Bloch waves with the assumption that the electron energy is $E(k) = \hbar^2 k^2/2m^*$ and m^* is energy-independent, where $\hbar$ is the Planck constant and m^* is an electron effective mass.

The k space elementary cell volumes for the RQW and QW are $(2\pi)^3/awL_z$ and $(2\pi)^3/L_xL_yL_z$,

respectively (as found in Ref. 2). Here, L_x, L_y, and L_z are the well dimensions. Thus, the corresponding (not normalized) state densities, $P(k)$, are

$$P_{\mathrm{RQW}}(k) = \frac{2awL_z}{(2\pi)^3}, \quad P_{\mathrm{QW}}(k) = \frac{2L_xL_yL_z}{(2\pi)^3}. \quad (1)$$

Factor 2 accounts for the spin. Thus, the normalized state densities are

$$\begin{aligned} \rho_{\mathrm{RQW}}(k) &= \frac{2}{(2\pi)^3}\frac{aw}{L_y(L_x+a/2)}, \\ \rho_{\mathrm{QW}}(k) &= \frac{2}{(2\pi)^3}. \end{aligned} \quad (2)$$

In Eq. (2), the real space volumes of the RQW and QW are considered, and we have introduced the geometry factor

$$G = \frac{L_y(L_x+a/2)}{aw}. \quad (3)$$

Thus, the comparison in Eq. (2) gives $\rho_{\mathrm{RQW}}(k) = \rho_{\mathrm{QW}}(k)/G$. The state density in k is reduced by factor G. The periodic lattice potential does not depend on QSD, and hence m^* and the dispersion relation $E(k)$ are identical for the RQW and QW. The state density in energy $\rho(E) = (dE/dk)^{-1}\,\rho(k)$ is reduced by the same factor G, i.e.

$$\rho_{\mathrm{RQW}}(E) = \frac{\rho_{\mathrm{QW}}(E)}{G}. \quad (4)$$

Subsequently, the concentration of the QSD-generated electrons n_{QSD} was determined. The quantum well layer was typically grown on a substrate of diverse band structures. A general case shown in Fig. 2 demonstrates that the band gaps of the substrate material are wider. The QSD takes place within the electron confinement intervals ΔE_j, where $j = 1,\ldots,4$. Each ΔE_j has the characteristic dispersion relation $E_j(k) = \hbar^2k^2/2m_j^*$ and density of states $\rho^{(j)}(E)$. Here, m_j^* is the electron effective mass within the jth interval. Inside each ΔE_j, there exist QSD-forbidden states, whose densities are

$$\begin{aligned} \rho^{(j)}_{\mathrm{FOR}}(E) &= \rho^{(j)}_{\mathrm{QW}}(E) - \rho^{(j)}_{\mathrm{RQW}}(E) \\ &= \rho^{(j)}_{\mathrm{QW}}(E)(1-G^{-1}), \end{aligned} \quad (5)$$

and Eq. (4) was used in Eq. (5). The total density of the forbidden states is the sum of the densities of the forbidden states from all intervals ΔE_j, i.e.

$$\begin{aligned} \rho_{\mathrm{FOR}} &= \sum_j \rho^{(j)}_{\mathrm{FOR}}(E) \\ &= (1-G^{-1})\sum_j \rho^{(j)}_{\mathrm{QW}}(E). \end{aligned} \quad (6)$$

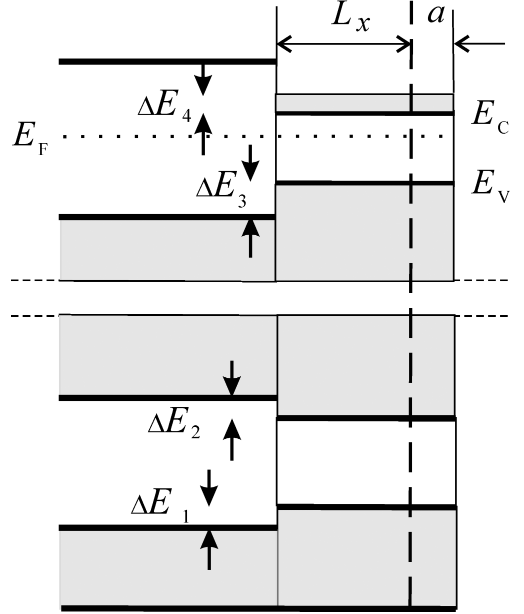

Fig. 2. Energy diagram of a semiconductor RQW grown on a wide band gap substrate.

The sum $\sum_j \rho^{(j)}_{\mathrm{QW}}(E)$ depends on the band structures of both the substrate and the RQW material, and can be calculated for a particular pair. Apparently, the sum does not depend on the QSD. Thus, the expression $n_{\mathrm{CON}} \equiv \sum_j \rho^{(j)}_{\mathrm{QW}}(E)$ is introduced, and the index shows that it is the electron-confinement-defined number. n_{CON} does not depend on the energy, since the summation by energy was already carried out. Thus, according to Eq. (6), the total number of forbidden quantum states (per unit volume) or the concentration of QSD-generated electrons can be rewritten as

$$n_{\mathrm{QSD}} = \rho_{\mathrm{FOR}} = n_{\mathrm{CON}}(1-G^{-1}). \quad (7)$$

Equation (7) gives the QSD doping. To calculate other RQW parameters, we used the condition of electrical neutrality,[6]

$$n_{\mathrm{RQW}} = p_{\mathrm{RQW}} + n_{\mathrm{QSD}} = p_{\mathrm{RQW}} + n_{\mathrm{CON}}(1-G^{-1}), \quad (8)$$

where n_{RQW} and p_{RQW} are the electron and hole concentrations in the RQW. They can be found using the semiconductor equation for the nondegenerate limit, as follows:

$$\begin{aligned} &n_{\mathrm{RQW}}p_{\mathrm{RQW}} \\ &\quad = \frac{N_C}{G}\frac{N_V}{G}\exp\left(-\frac{E_g}{K_BT}\right) = \frac{n^2_{\mathrm{QW}}}{G^2} = n_i^2. \end{aligned} \quad (9)$$

Here, N_C and N_V are the effective state densities in the CB and VB of the QW, $E_g = E_c - E_v$ is the band gap width, K_B is Boltzmann's constant, T is

the absolute temperature, $n_{\rm QW}$ is the electron concentration in the QW, and n_i is the initial (to QSD doping) electron concentration in the RQW. To obtain Eq. (9), we divided the state densities by a factor G according to Eq. (4), and used the semiconductor equation for the conventional QW, $n_{\rm QW}^2 = N_C N_V \exp(-E_g/K_B T)$. The combination of Eq. (8) and Eq. (9) gives

$$n_{\rm RQW} = \frac{1}{2G}\left\langle n_{\rm CON}(G-1) + \left[n_{\rm CON}^2(G-1)^2 + 4n_{\rm QW}^2\right]^{1/2}\right\rangle, \quad (10)$$

where $n_{\rm RQW}$ is similar to $n_{\rm QW}$ in the limits of QSD absence. The first limit is $G = 1$ (no state density reduction). Equation (10) shows that for $G = 1$, $n_{\rm RQW} = n_{\rm QW}$. Another limit is $n_{\rm CON} = 0$ (no confinement), in which Eq. (10) gives $n_{\rm RQW} = n_{\rm QW}/G$, where the latter is not similar to $n_{\rm QW}$ for any value of G. Divergence is apparent, since G can have only one value of $G = 1$ in the case of zero confinement. Actually, $n_{\rm CON} = 0$ corresponds to no boundaries and no RQW geometry. $p_{\rm RQW}$ can be obtained from Eqs. (10) and (9).

Subsequently, we determined the increase in E_F due to QSD doping ΔE_F. We used the formula $\Delta E_F = k_B T \ln(n_{\rm RQW}/n_i)$ for the nondegenerate limit.[6] By inserting $n_{\rm RQW}$ from Eq. (10) and n_i from Eq. (9), we get

$$\Delta E_F = k_B T \ln\left\langle \frac{n_{\rm CON}(G-1)}{2n_{\rm QW}} + \left[\frac{n_{\rm CON}^2(G-1)^2}{4n_{\rm QW}^2} + 1\right]^{1/2}\right\rangle. \quad (11)$$

Figure 3 demonstrates the ΔE_F dependence on $n_{\rm CON}$ for some values of G according to Eq. (11). ΔE_F is most sensitive to changes in G for a low G values ($G \approx 1$). For $G > 3$, the dependence is less sensitive to changes in G and is linear in the logarithmic scale. Such behavior is natural, as for G somewhat exceeding unity, the state density remains high and a small increase in the value of G generates a large number of QSD-rejected electrons. On the contrary, for $G > 3$, the state density is reduced dramatically, and further increase in G does not generate that many rejected electrons. In addition, ΔE_F will further increase for $(n_{\rm CON}/n_{\rm QW}) > 10^5$. However, we do not extend the curves, since Eq. (11) is true only within the nondegenerate limit. In the case of higher $n_{\rm CON}/n_{\rm QW}$, when the semiconductor becomes degenerated, Fermi integrals should be used to calculate $n_{\rm RQW}$ and ΔE_F. However, this could be done only within the limited energy range near the bottom of the CB, since the above analysis is true only in the approximation that m^* is energy-independent.

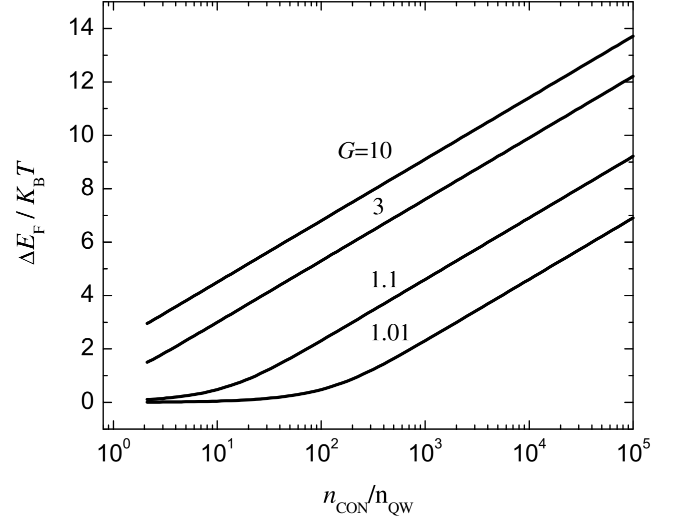

Fig. 3. Fermi energy increase as the function of QSD doping for some values of G.

Charge carrier scattering rates are proportional to $\rho(E)$ according to Fermi's golden rule and are reduced in the RQW. If τ is the carrier transport lifetime, then according to Eq. (4) we have $\tau_{\rm RQW} = G\tau_{\rm QW}$. Consequently, for mobility $\mu = e\tau/m^*$, we get

$$\mu_{\rm QW} = G\mu_{\rm QW}\,. \quad (12)$$

The mobility of charge carriers increases G times in the RQW. In the case of heavy QSD doping ($n_{\rm RQW} \gg p_{\rm RWQ}$), the hole current can be neglected and the electrical conductivity using Eq. (12) in Eq. (13) is given as

$$\sigma_{\rm RQW} = e\mu_{\rm RQW} n_{\rm RQW} = \sigma_{\rm QW} G(n_{\rm RQW}/n_{\rm QW})\,. \quad (13)$$

Furthermore, by inserting Eq. (10) in Eq. (13), we get

$$\sigma_{\rm RQW} = \sigma_{\rm QW}\left\langle \frac{n_{\rm CON}(G-1)}{2n_{\rm QW}} + \left[\frac{n_{\rm CON}^2(G-1)^2}{4n_{\rm QW}^2} + 1\right]^{1/2}\right\rangle. \quad (14)$$

Equation (14) indicates that the conductivity of the RQW increases with respect to the QW. Figure 4 shows the conductivity dependence on

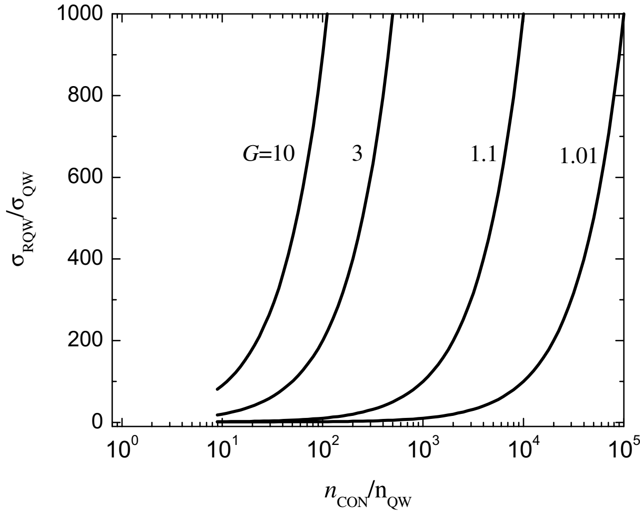

Fig. 4. Conductivity dependence on QSD doping for some values of G.

QSD-generated electron concentration for some values of G. In the general case, the hole current contributes to the mechanism and should be included in Eq. (13), and can be calculated in a similar way using p_{RQW} determined from Eqs. (10) and (9).

3. Geometry Factor Calculation

The conventional QW ($a = 0$) has quasi-2D structure $L_y, L_z \gg L_x$, and no quantum features are considered in the Y and Z directions. Nonnormalized state density is $P(E) = \rho(E)L_xS$, where S is a layer surface and $P(E)$ is proportional to the product $\rho(E)L_x$. As $\rho(E)$ in the RQW is reduced G times, L_x can be similarly increased with respect to G times without the loss of quantum properties. Let us find G for the arbitrary geometry. There are no analytical solutions to the time-independent Schrödinger equation in the ridged well (the solution contains infinite sums). However, there are fairly accurate mathematical and numerical methods. Mathematically, there is no difference between QSD and electromagnetic mode depression, and the Helmholtz equation and the same boundary conditions are used in both the cases. Helmholtz spectrum calculation can be found in the literature related to Casimir effect. Casimir energy exhibits strong dependence on the photon spectrum and, consequently, on the geometry of the vacuum gap.[7] A number of geometries, including double-side ridged geometry[8] and double-side corrugated geometry,[9] were analyzed. A new, optical approach for arbitrary geometry was also developed.[10] In addition, a software program designed for wave mode calculation in ridged waveguides has been developed,[11,12] and can be used to determine G numerically.

In practice, $w \gg a$, which allows the assumption that the k spectrum is quasi-continuous in the Y direction. Thus, in the first approximation, G can be rewritten in a simpler form:

$$G = \frac{L_x + a/2}{a} \approx \frac{L_x}{a}. \qquad (15)$$

In Eq. (15), we consider that $a \ll 2L_x$, which is satisfied automatically within the perturbation method limit [Eq. (3) is obtained using the perturbation method]. We presume that this method is precise enough in the range of $5 < (L_x/a) < 10$, and Eq. (15) can be used for that range (the method cannot be used for $a \to 0$, since diffraction leads to ignoring the ridges by wave). Therefore, we used the values of $G = 5$–10 for further estimations. In practice, a 20-nm-wide conventional QW can be replaced by a 100–200-nm-wide RQW.

4. Possible Applications

For optoelectronics and power electronics, it is important to have suitable wide band gap materials.[13] Semiconductors with $E_g > 1.5\,\mathrm{eV}$ are difficult to employ, as their electrical conductivity is low. Hence, donor doping is typically used to increase the conductivity. However, conventional doping introduces impurity centers and increases electron scattering, and thus the QSD doping can be used to solve these problems. It increases the electron concentration in the CB without introducing scattering centers. Besides, the QSD increases the carrier mobility in both the CB and the VB.

The QW embedded in the *p–i–n* junction is frequently used for solar cells,[14,15] semiconductor lasers,[16] and infrared detectors.[17] A typical QW layer is only 10–20-nm thick, and thus there exists the problem of light confinement. To overcome this, complicated multiple QW heterostructures are fabricated. The QSD can contribute in difficulty solving. The RQW layer has the same quantum properties at G times more thickness, and increases the light confinement. Hence, a reduced number of RQW layers will be required. In addition, the combination of the QW and RQW can be used for solar cells.

Ballistic MOSFETs are widely discussed in the literature.[18–20] The ballistic regime is difficult to realize in practice, because of the low mean free

path (5–10 nm) of charge carriers. Using the RQW in the transistor channel reduces the scattering rates, and consequently increases the mean free path to G times, for both electrons and holes.

Molecular beam epitaxy (MBE) is typically used to grow QW layers. RQW growth does not differ from conventional QW growth, except that the RQW layer has more thickness. Thus, it becomes simpler to fabricate from the point of thickness accuracy. Since the RQW is hundreds of nanometers thick, different fabrication methods can also be used; for example, silicon-on-insulator (SOI) technology can be utilized to cleave and bond layers of that thickness.[21] SOI allows mechanical attachment of the RQW layer to the substrate, instead of growing it using complicated MBE technology.

5. Conclusions

The QSD in a semiconductor RQW was investigated. This study demonstrated that the QSD reduces the density of quantum states by geometry factor G, and the electrons from the filled energy bands are transferred to the empty ones. The electron concentration in the CB increases and corresponds to the donor doping. The QSD doping does not introduce impurities, but increases the carrier mobility to G times.

Formulas for carrier concentrations and E_F were obtained in the nondegenerate limit. It was observed that the methods developed for Casimir energy calculation in complicated geometries can be utilized to obtain the precise value of G.

The RQW exhibited quantum properties at G times more width with respect to the conventional QW. This can be used in various applications in optoelectronics, the RWQ can increase the light confinement and reduce the number of layers; and in MOS transistors, the RQW can improve the ballistic properties.

Acknowledgments

The authors are grateful to A. Bibilashvili for useful discussions. This work was supported by Borealis Technical Limited, assignee of the corresponding U.S. patents (7,220,984; 7,166,786; 7,074,498; 6,281,514; 6,495,843; 6,680,214; 6,531,703; and 6,117,344).

References

1. H. Davies, *The Physics of Low-Dimensional Semiconductors* (Cambridge University Press, 1998).
2. A. Tavkhelidze, V. Svanidze and I. Noselidze, *J. Vac. Sci. Technol. B* **25**, 1270 (2007).
3. A. Tavkhelidze, A. Bibilashvili, L. Jangidze, A. Shimkunas, P. Mauger, G. F. Rempfer, L. Almaraz, T. Dixon, M. E. Kordesch, N. Katan and H. Walitzki, *J. Vac. Sci. Technol. B* **24**, 1413 (2006).
4. V. M. Sedykh, *Waveguides with Cross Section of Complicated Shape* (Kharkhov University Press, 1979), p. 16.
5. W. S. C. Chang, *Principles of Lasers and Optics* (University of California, San Diego, 2005).
6. S. M. Sze, *Physics of Semiconductor Devices* (Wiley-Interscience, 1981).
7. T. Emig, A. Hanke, R. Golestanian and M. Kardar, *Phys. Rev. Lett.* **87**, 260402 (2001).
8. R. Büscher and T. Emig, *Phys. Rev. Lett.* **94**, 133901 (2005).
9. R. B. Rodrigues, P. A. Maia Neto, A. Lambrecht and S. Reynaud, *Europhys. Lett.* **76**, 822 (2006).
10. A. Scardicchio and R. L. Jaffe, *Nucl. Phys. B* **704**, 552 (2005).
11. FIMMMWAVE, photon design software (a fully vectorial 2D mode solver), http://www.photond.com/products/fimmwave.htm
12. CONCERTO, software for electromagnetic design, Vector Fields, http://www.vectorfields.com
13. Y. C. Choi, J. Shi, M. Pophristic, M. G. Spencer and L. F. Eastman, *J. Vac. Sci. Technol. B* **25**, 1836 (2007).
14. D. B. Bushnell, T. N. D. Tibbits, K. W. J. Barnham, J. P. Connolly, M. Mazzer, N. J. Ekins-Daukes, J. S. Roberts, G. Hill and R. Airey, *J. Appl. Phys.* **97**, 124908 (2005).
15. J. C. Rimada, L. Hernández, J. P. Connolly and K. W. J. Barnham, *Microelectron. J.* **38**, 513 (2007).
16. K. Okamoto, H. Ohta, S. F. Chichibu, J. Ichihara and H. Takasu, *Jpn. J. Appl. Phys.* **46**, L187 (2007).
17. H. Son, J. Park, S. Hong, S.-J. Jo and J.-I. Song, *Appl. Phys. Lett.* **79**, 455 (2001).
18. K. R. Shanbhag and P. C. Subramaniam, in *Int. Workshop on Physics of Semiconductor Devices*, 2007, pp. 257–260.
19. M. H. Liao and C. W. Liu, *Appl. Phys. Lett.* **92**, 063506 (2008).
20. K. Likharev, in *Nano and Giga Challenges in Microelectronics*, eds. J. Greer *et al.* (Elsevier, Amsterdam, 2003), p. 27.
21. O. Moutanabbir, B. Terreault, N. Desrosiers, A. Giguère, G. G. Ross, M. Chicoine and F. Schiettekatte, *AIP Conf. Proc.* **772**, 1491 (2005).